Table 8. Bolded E_p's are in the range 1965.2-3048 cm^{-1}. These E_p's are used to construct Table 9 and Figs.13 and 14.

n_i	Comments	n_f = 4	Comments	n_f = 5	Comments	n_f = 6	Comments	n_f = 7
5	Inner&OuterBring&**[26]**	***2469.1***						
6	(high E_p's)	3810.3	(low E_p)	1341.2				
7	↓	4619.0	**[2, 23, 24]**	***2149.9***	(low E_p)	808.7		
8		5143.9	**[27]**	***2674.8***	(low E_p)	1333.6	(low E_p's)	524.9
9		5503.8	**[28]**	***3034.7***	(low E_p)	1693.5	↓	884.8
10		5761.2	(high E_p's)	3292.1	(low E_p)	1950.9		1142.2
11		5951.6	↓	3482.6	**[2, 23, 24]**	***2141.3***		1332.6
12		6096.5		3627.4	Dring&InnerBring&[**20**]	***2286.2***		1477.5
13		6209.2		3740.1	Dring&InnerBring&[**21**]	***2398.9***		1590.2
14		6298.7		3829.6	Dring&Inner&OuterBrings	2488.4		1679.6
15		6370.8		3901.8	Dring&Inner&OuterBrings	2560.5		1751.8
16		6429.9		3960.8	D ring	2619.6		1810.9
17		6478.8		4009.8	D ring	2668.5		1859.8
18		6519.9		4050.8	D ring	2709.6	↑	1900.8
19		6554.6		4085.5	D ring	2744.3	(low E_p's)	1935.6
20		6584.2		4115.1	D ring	2773.9	A ring **[3]**[1]	***1965.2***
21		6609.7		4140.6	D ring	2799.4	A ring	1990.7
22		6631.8		4162.8	D ring	2821.5	A ring	2012.8
23		6651.1		4182.0	D ring	2840.8	A ring	2032.1
24		6668.0		4199.0	D ring	2857.7	A ring	2049.0
25		6683.0		4213.9	D ring	2872.7	A ring	2064.0
26		6696.2		4227.1	D ring	2885.9	A ring	2077.2
27		6708.0		4238.9	D ring	2897.7	A ring	2089.0
28		6718.6		4249.5	D ring	2908.3	A ring	2099.6
29		6728.1		4259.0	D ring	2917.8	A&C rings	2109.0
30		6736.6		4267.6	D ring	2926.3	A&C rings	2117.6
31	↑	6744.4	↑	4275.3	D ring	2934.1	A&C rings	2125.3
32	(high E_p's)	6751.4	(high E_p's)	4282.3	D ring	2941.1	A&C rings	2132.4
∞	(high E_p)	6858.6	high E_p	4389.5	**[29]**	***3048.3***	[**1, 22, 25]**	***2239.5***

[1]Daphnis is in the Keeler Gap near the outer edge of the A ring. NASA(2021)

Notes: E_p's used for Fig. 13. are in the range (1965.2-3048.3 cm^{-1}) corresponding to the outer edge of the A ring to the inner edge of the D ring. (high E_p's) and (low E_p's) are not in this range.

The comment columns contain the indices [*i*]*'s* used in Tables 6, 7, 8, 9 and Figs 12 and 13.

Other comments connect certain E_p's with the A, B, C and D rings.

Bolded E_p's with [*i*]'s associated with them are the key E_p's in Fig.13.

The center of the B ring is near the peak in the PED of Saturn's protosatellite disk.

The inner B ring exists to the left of this peak in Fig. 13.

The outer B ring exists to the right of this peak in Fig. 13.

Table 9. Photon energies (E_P's) and orbital radii (r/R_s) used for the construction of Figs. 13,16,17 and 18. The individual pairings of E_p's and r/R_s's are determined by first pairing Ep(7,∞) with the inner radius of the A ring and the inner and outer radius of the C ring. Then the other pairings automatically fall into place.

Satellite or Ring Edge Name	[*i*][a]	r/R_s [b]	n_f, n_i [c]	$E_p(n_f, n_i)$ [c] (cm^{-1})
Saturn's Equatorial radius		1.000		
Inner Edge D ring	[29]	1.110	6,∞	3048.3
D68 ringlet	[28]	1.122[d]	5,9	3034.7
D72 ringlet	[27]	1.187[d]	5,8	2674.8
D73 ringlet	[26]	1.216[d]	4,5	2469.1
Outer Edge D ring		1.236		
Inner Edge C ring	[25]	1.239	7,∞	2239.5
Titan ringlet in Colombo Gap	[24]		5,7	2149.9
Titan ringlet in Colombo Gap	[24]		6,11	2141.3
Average Titan ringlet E_p's	[24]	1.292		2145.7
Maxwell ringlet in Maxwell Gap	[23]		6,11	2141.3
Maxwell ringlet in Maxwell Gap	[23]		5,7	2149.9
Average Maxwell ringlet E_p's	[23]	1.452		2145.7
Outer Edge C ring	[22]	1.526	7,∞	2239.5
Inner Edge B ring		1.526		
Outer Edge B ring		1.950		
Huygens ringlet in Huygens Gap	[21]	1.955[e]	6,13	2398.9
Laplace ringlet in Laplace Gap	[20]	1.992[e]	6,12	2286.2
Inner Edge A ring	[1]	2.030	7,∞	2239.5
Pan in Encke Gap	[2]		5,7	2149.9
Pan in Encke Gap	[2]		6,11	2141.4
Average Pan E_p's	[2]	2.217		2145.7
Daphnis and Keeler Gap	[3]	2.265	7,20	1965.2
Outer Edge A ring		2.270		

[a] Indices in Tables 7, 8 and 9 & Figs. 12, 13 and 15.

[b] Orbital radii of satellites and rings in units of the equatorial radius of Saturn and from NASA (2021) except as otherwise noted. These orbital radii are transformed with Eq. (8) to give $(r/R_s)'$ values used in Fig. (18).

[c] The quantum numbers that define transitions in the hydrogen atom and photon energies associated with these transitions.

[d] Hedman et al. (2007b)

[e] French et al. (2020) their Fig. 2 and NASA (2022)

Fig. 13. The Photon Energy Distribution in Saturn's protoplanetary disk, highlighting the A, B, C and D rings & the Cassini Division

Figure 13

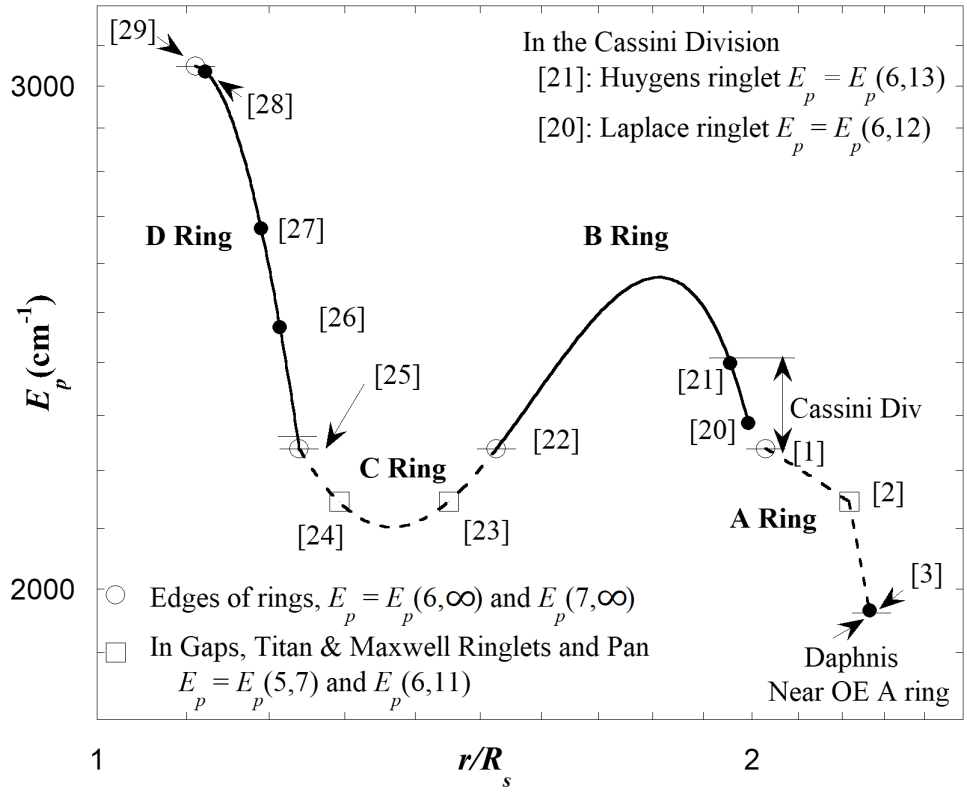

radii of the D ring are the distinctive features of the ring. Furthermore Table 8 reveals there are just three bolded E_p's that fall within the D ring. These E_p's are associated with the three ringlet radii. Figure 13 shows the resulting PED from index [22] to index [29] to be a smooth curve that defines a dip in the PED of Saturn's protosatellite disk.

2.7.c. The B Ring, Cassini Division and Resonance Ring Widths

In the present model resonance rings overlap within the rings of Saturn but not outside. The width of resonance rings within the wide rings undoubtedly depend on a few factors, e.g. the local temperature gradient, and the dust and gas densities in the rings. The variability in these factors could explain why the inner edge of the B ring extends inward all the way to the outer edge of the C ring while the outer edge does not extend outward all the way to the inner edge of the A ring, and the Cassini Division exists between the A and B rings. On average the optical depth of the Cassini Division is low (French et al. 2020), but it is not completely void of material and there are eight gaps (Planetary Society 2021) in the Cassini Division. Among these are the Laplace and Huygens Gaps each with a ringlet within its boundaries.

The optical depth of the two ringlets is large and the ringlets are narrow compared to the other features in the Cassini Division, as seen in the optical depth profile of the Cassini Division (French et al. 2020 Fig. 2 & Jerousek et al. 2020 Fig.1), and the ringlets therefore are the dominant features in the Cassini Division. In Table 8 there are just two E_p's, $E_p(6,12)$ and $E_p(6,13)$, that have values corresponding to the Cassini Division and they are paired with the Laplace [20] and Huygens [21] ringlets in Table 9 and Figs. 13 and 14. The width of these ringlets are about 40 and 20 km respectively and the difference in their radii is about 2,200 km (French et al. 2020 Fig. 2).

Fig. 14. The PED in the B ring and Cassini Division with the middles of resonance rings indicated as well as quantum numbers of corresponding E_p's

Figure 14

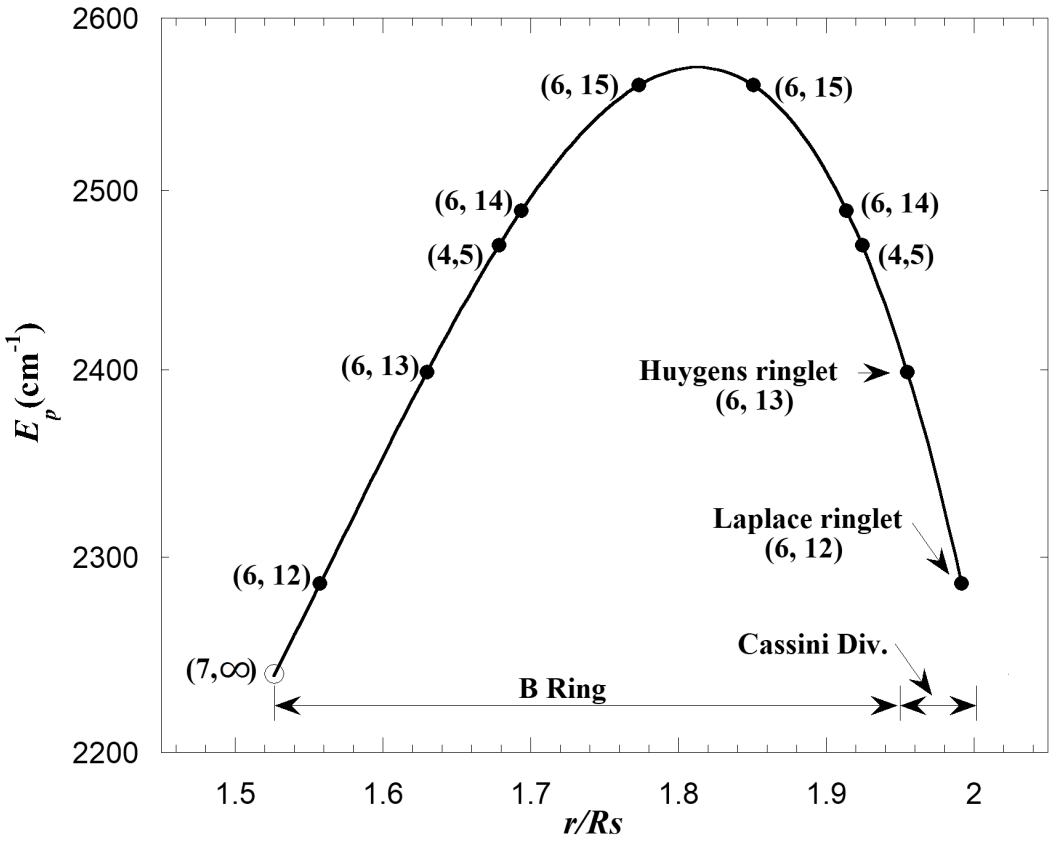

The peaked solid curve in Fig. 13 approximates the PED in the region of the B ring and Cassini Division. It is determined as described in Appendix 4. In this approximation the peak value in the PED is slightly larger than $E_p(6,15)$. Therefore $E_p(6,15)$ is the largest E_p value contributing to the B ring as indicated in Table 8. Using Table 8 and Fig. 14, we can count the number of just barely overlapping resonance rings that create the B ring by counting the E_p's that create resonance (Three of them are counted twice). Starting from the inner edge of the B ring and moving outward to the outer edge we have $E_p(6,12)$, $E_p(6,13)$, $E_p(4,5)$, $E_p(6,14)$, $E_p(6,15)$, $E_p(6,15)$, $E_p(6,14)$, $E_p(4,5)$: 8 overlapping resonance rings. Assuming these rings barely overlap, the average width of a resonance ring would be

approximately 1/8th the width of the B ring or approximately 3200 km. This is about 100 times wider than the Laplace and the Huygens ringlets in the Cassini Division where the optical depth is low.

In Table 8, [26] is paired with $E_p(4,5)$ and this resonance causes a ringlet in the D ring. We might expect photons with energy $E_p(4,5)$ to affect the B ring in the same way they affect the D ring. If this were the case, there would be two ringlets corresponding to the $E_p(4,5)$ resonance also observed in the B ring with one on each side of the PED peak. The lack of these ringlets is likely related to the larger density of material that presumably existed in the B ring over the D ring when resonance rings existed. Presently the optical depths of the B and D ring are 0.4-2.5 and 10^{-5} respectively (NASA 2021).

2.8. The Temperature Distribution in Saturn's Protosatellite Disk

Mousis, Gautier and Bockelee-Moran (2002) (in the future referred to as MGB) have theoretically derived a series of six TD's for the Saturnian subnebula (protosatellite) disk. Their TD's are shown in their Fig. 1. The first four of these are reproduced in Fig. 15. (The reproduction is achieved by analyzing coordinates of points on the MGB TD curves with the photo editor GIMP). We now investigate the relationship between the MGB TD's and the E_p's and r/R_s values listed in Table 7.

Fig. 15. Reproduction of TD's in Saturn's protosatellite disk*

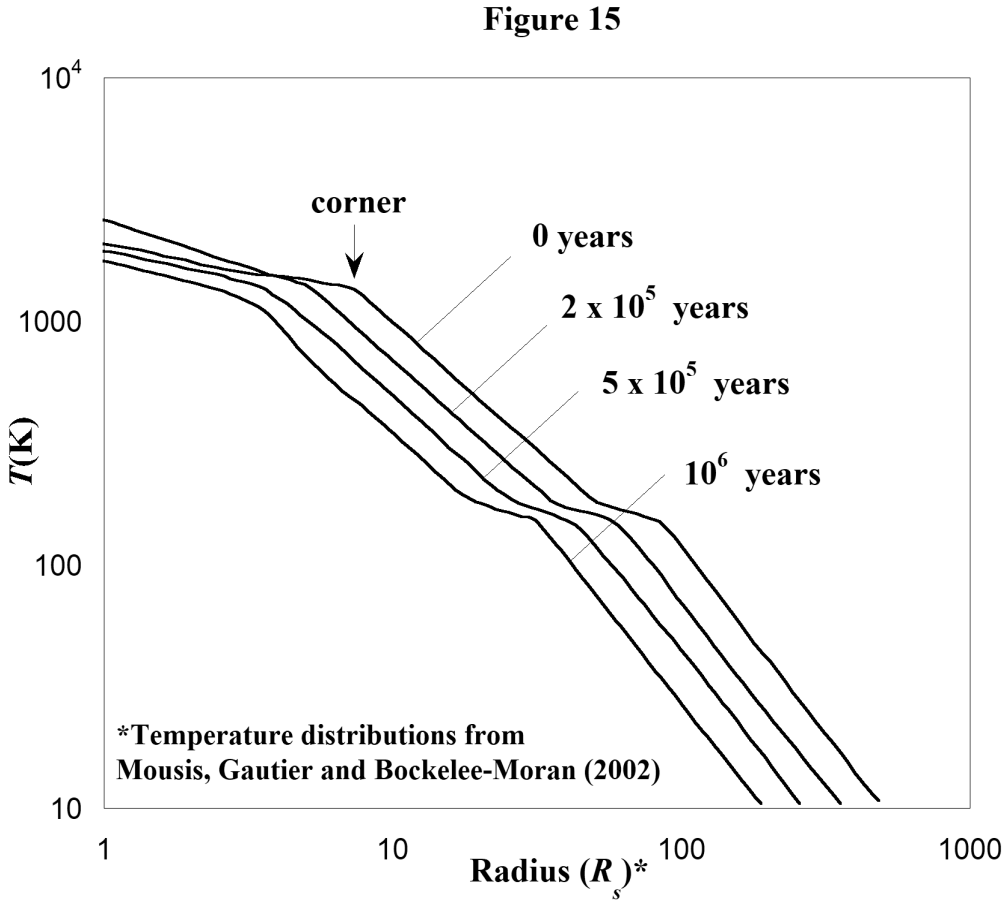

As in section 2.3.b for Uranus, we assume Saturn's rings and regular satellites evolved from primordial rings that were born in the Saturnian protosatellite disk with each primordial ring associated with the local mid-plane temperature T of the disk. Each of these T's is related to one of the E_p values previously discussed for the Saturnian disk. We again assume the relationship between T and E_p is linear and of the form

$$T = C'_1(E_p + C'_2), \qquad (7)$$

where C'_1 and C'_2 are constants to be empirically determined. To determine these constants we use Eq. (7) with the r/R_s values and E_p's in Table 7. A trial set of C'_1 and C'_2 is used to calculate a T for each E_p in Table 7. Then these T's and their corresponding values of r/R_s are used to construct a trial TD. This TD is compared to the TD curves in Fig. 15. After many iterations it is determined that no good fit can be found to any of the MGB TD's. Fig. 16 shows the fit to the MGB TD for which t = 5 x 10^5 years.

Fig. 16. Fitting the Saturnian disk TD to the MGB TD for which t = 5 x 10 years. The fit is not as good as the one in Fig. 17.

Figure 16

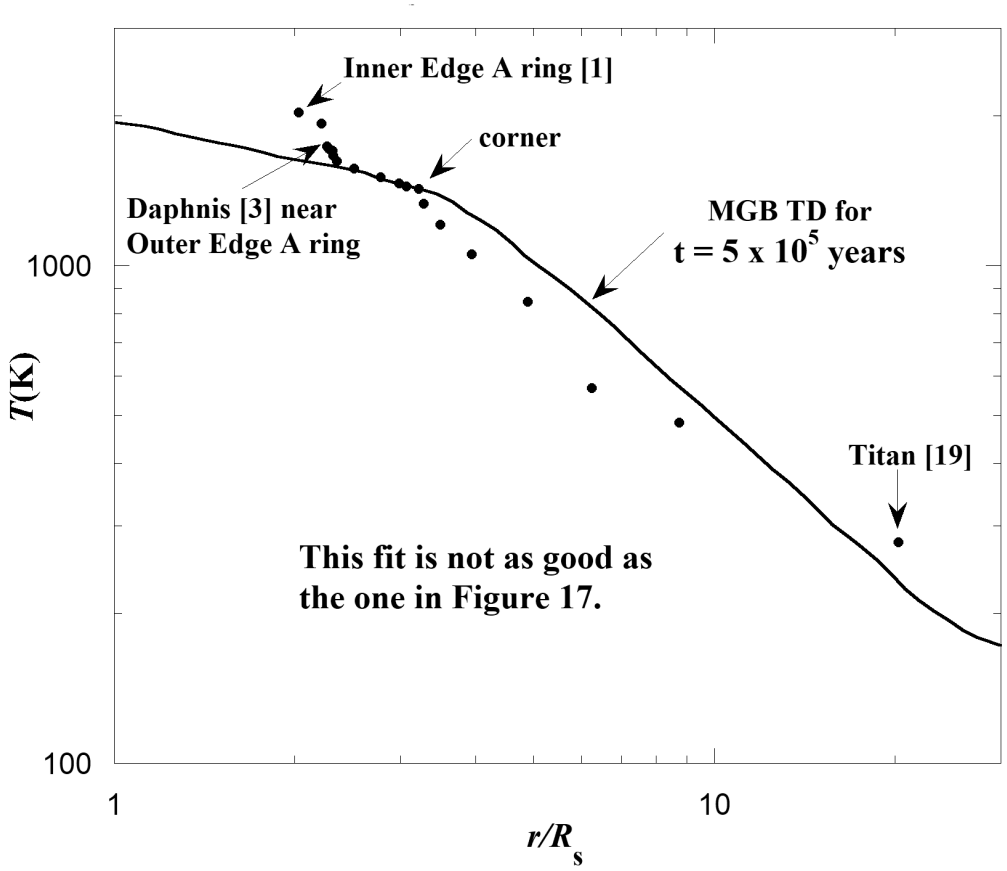

The fit is not good but the shape of the trial TD (the collection of data points) gives a hint on how to proceed. A corner in the trial TD is identified in Fig. 16. And notice the MGB TD for which t = 0 in Fig. 15 also has a corner. Perhaps these corners can be made to overlap and hopefully this will produce